



## Green Synthesis and Characterization of Nickel Oxide Nanoparticle for Rhodamine-B Adsorption using *Phyllanthus emblica* Fruit Extract

P.S. GEETHA MALINI<sup>1,2</sup>, S. RANI<sup>3,\*</sup>, J. MANONMANI<sup>1</sup> and R. JAYAPRAKASH<sup>4</sup>

<sup>1</sup>Department of Chemistry, Quaid-E-Millath Government College for Women, Chennai-600002, India

<sup>2</sup>Department of Chemistry, Sri Chandrasekharendra Saraswathi Viswa Mahavidyalaya, Enathur, Kanchipuram-631561, India

<sup>3</sup>PG & Research Department of Chemistry, Arignar Anna Government Arts College, Cheyyar-604407, India

<sup>4</sup>Department of Chemistry, School of Arts and Science, AV Campus, Vinayaka Mission's Research Foundation (Deemed to be University), Chennai-603104, India

\*Corresponding author: E-mail: raniselvaraj1970@gmail.com

Received: 22 January 2023;

Accepted: 1 March 2023;

Published online: 30 March 2023;

AJC-21196

In this work, the nanoadsorbent efficiency of nickel oxide nanoparticles (NiONPs) for the degradation of rhodamine B (RhA-B) dye was examined. The NiONPs were synthesized by green technique using  $\text{NiCl}_2 \cdot \text{H}_2\text{O}$  and *Phyllanthus emblica* fruit extract. The NiO nanoparticles were characterized using UV, FTIR, FESEM, HRTEM and TGA/DTA analysis to study the decomposition pattern, functional groups, crystalline size and elemental composition of nanoparticles. TEM analysis showed that the nanoparticles were spherical, highly crystalline, highly agglomerated and appeared as clusters of nanoparticles in the size range converted into tubular shape. The prepared NiONPs were used for batch experiments to evaluate the adsorption capacities of the dye. The influence of various key parameters, i.e. adsorbent dosage and initial dye concentration were investigated. The extent of adsorption of RhA-B was found to be 88% at pH 6. Langmuir isotherm showed maximum monolayer adsorption with  $q_m$  values from 328–465 mg/L. The kinetic investigation of RhA-B degradation followed a pseudo-second-order rate kinetics with a rate constant of  $2.0495 \times 10^{-3} \text{ mg}^{-1} \text{ min}^{-1}$ .  $\Delta G^\circ = -79.00 \text{ kJ/mol}$  indicates that the adsorption is chemisorption and spontaneous.

**Keywords:** NiO, *Phyllanthus emblica*, Nanoparticles, Rhodamine B dye, Adsorption.

### INTRODUCTION

The textile, leather, paper, printing, plastic, culinary, cosmetic, photographic and pharmaceutical industries are the most prolific offenders in terms of dye consumption and their practices inevitably lead to water decolorization [1,2]. Due to environmental discharge pressure, hazardous chemical effluents have received more attention [3,4]. Even trace colours and pigments in effluents are hazardous. Rapid industrialization can boost the economy, but it can also reduce photosynthesis in streams and diminish the water's aesthetic value. It's dangerous since it can irritate people's skin, stomachs, lungs and eyes. These are just some of the reasons why it's so important to clean up dye effluents before they're dumped into rivers or the ocean [5]. Therefore, the process of removing colours from textile effluent is of great interest to scientists all over the world.

In recent years, dye-containing wastewater has been treated via reverse osmosis, coagulation, coagulation-flocculation,

electrocoagulation, chemical oxidation, solvent extraction, ion exchange and adsorption [6]. Because of low treatment costs, ease of construction and operation and efficient treatment of effluents, adsorption has become a popular alternative to more conventional methods of wastewater purification [7,8]. The efficiency of adsorption is dependent on the capacity of the adsorbents used. On the downside, the efficiency with which these materials adsorb is poor [9]. This highlights the need for improved adsorbents to overcome the issues. Nanoscience and nanotechnology are shown to be most successful in solving environmental concerns [10]. Nanostructured adsorbents, largely due to their extremely large surface area, exhibit significantly greater efficiency and quicker adsorption than traditional materials [11,12]. Carbon-based nanomaterials like activated carbon, carbon nanotubes and graphene are the most investigated for wastewater treatment [13]. They can be processed into many different shapes, including particles, rings, tubes and sheets. Other inorganic nanoparticles used for removing

dyes and heavy metal ions are based on metals or metal oxides. Because of their low toxicity, insolubility and lack of involvement in the generation of secondary pollutants, metal oxides have found widespread use as sorbents for the elimination of toxic chemicals such as heavy metals and synthetic colours. According to the literature, there are numerous approaches to obtain nickel oxide nanoparticles (NiONPs). Spray pyrolysis, combustion, sol-gel, co-precipitation and the anode arc plasma technique are all names for this process [14,15]. The current work reports on a simple green synthesis, which has advantages over previous approaches because it is highly simple, rapid and eco-friendly [16-18]. In this study, NiONPs were prepared using nickel chloride and *Phyllanthus emblica* extract in a green synthesis process. The UV, FTIR, FE-SEM, HR-TEM and thermal analysis were used to characterize the obtained NiONPs. Investigations were made with different parameters including adsorbate concentration and adsorbent dosage. The uptake process was explained using the concepts of kinetics, adsorption isotherms and thermodynamic parameters.

## EXPERIMENTAL

All chemicals were purchased from Sigma-Aldrich, India and used without further purification. *Phyllanthus emblica* fruit were collected from the local garden of Tiruvetipuram, Tiruvannamalai District, South India.

**Preparation of *Phyllanthus emblica* fruit extract:** *P. emblica* fruit were dried, grinded as a powder and then treated with 100 mL of distilled water, which was then agitated for 8 h on low heat. Each batch was filtered through eight layers of muslin cloth and centrifuged at 5000 rpm for 15 min every 2 h. After two filtrations, the supernatant was collected, cooled and concentrated using a rotating vacuum evaporator at low pressure. The extracted concentrate was pasteurized and preserved at 4 °C [19]. The prepared extract was carried to prepare the NiONPs.

**Preparation of nickel oxide nanoparticles:** Nickel oxide nanoparticles were synthesized by the green technique using nickel chloride hexahydrate (NiCl<sub>2</sub>·6H<sub>2</sub>O) and surfactant. To a mixture of 0.5 mol of nickel salt with 2% of surfactant, 10% (wt./vol.) *Phyllanthus emblica* fruit extract was added slowly and heated to 70 °C (NiO-70) with continuous agitation for 1 h [20]. After the heating, the precipitate was washed many times and dried in a vacuum oven at 70 °C. This research obtained 65% yield of nanoparticles and preserved in sealed container. Each 5 g of NiONP-70 was calcinated at different temperatures such as 200, 400 and 600 °C in a muffle furnace for 1 h separately. They were designated as NiO-200, NiO-400 and NiO-600, respectively.

**Preparation of RhA-B dye solution:** A 1000 mg/L stock solution of RhA-B dye was diluted with distilled water to obtain dye solutions of various concentrations ranging from 10 mg/L to 100 mg/L.

**UV and FTIR analysis:** For this study, a UV-visible spectrometer was used to examine the UV-absorption spectra of NiONPs produced with *Phyllanthus emblica* fruit extract (Shimadzu UV-2700). From the absorption spectra, Tauc plot was plotted and the energy gap was calculated for the different temperature treated NiONPs. The band gap (energy) of the

NiONPs was determined by using a well-known relation given by Tauc plot. This was done by analyzing the absorption spectra using eqn. 1:

$$(\alpha h\nu)^{1/n} = A(h\nu - E_g) \quad (1)$$

where  $\alpha$  is the absorption coefficient; A is the energy independent constant; h is the Planck constant; n is the direct band gap (=1/2) and  $E_g$  is the indirect band gap (=2), respectively.

The synthesized NiONPs vibrational spectroscopy (FTIR) recorded in Bruker model from 4000 to 400 cm<sup>-1</sup> using KBr pellet.

**Surface morphology:** Morphological analysis was performed by means of a scanning electron microscope equipped with a field emission FE-SEM by using FEI-Quanta FEG 200F model. TECHNAI 10 Philips was used to capture the TEM images of the obtained NiONPs. After sonicating NiONPs for 5 min, a diluted sample was deposited in a drop on a carbon-coated copper grid for examination. The vapourization of the liquid component took place at ambient temperature.

**Thermal analysis (TGA and DTA):** On a Hi-Res SDT 2960 model thermal analyzer, both thermogravimetric analysis (TGA) and differential thermal analysis (DTA) were carried out. Carrier gas consists of dry air. The temperature ramp for TGA and DTA was 10 °C per min and the temperature range exists between 20 °C and 60 °C.

**Effect of NiONPs dosage:** From the characterization of four types nanoparticles (NiO-70, NiO-200, NiO-400 and NiO-600), this work observed that NiO-600 was more homogeneous and had smaller spherical nanoparticles. Because of this, organic dye RhA-B had to be removed from the aqueous solution and NiO-600 was used as an adsorbent at pH = 6. The prepared NiONPs-600 was treated with dye RhA-B and analyzed the adsorption tendency with respect of nanoparticle surface.

**Effect of RhA-B dye concentration:** Similarly, the study was carried using constant NiONPs quantity with the serially diluted dye concentrations between 10 and 100 ppm.

**Adsorption studies:** Various adsorption experiments were carried out in batch mode at 30 °C in this study. In order to obtain standards for each experiment, a predetermined amount of adsorbent was placed inside of each Erlenmeyer flask. To ensure consistent mixing throughout the experiment, agitation was performed at a rate of 200 rpm for each run. Before swirling the contents of each flask, a measured amount of sample was poured in each vessel (an adsorption solution with an initial concentration ranging from 10-100 mg/L). At predetermined times, shaker flasks containing samples were withdrawn from the apparatus. In order to obtain the adsorption-desorption equilibrium and analyze the adsorption of rhodamine B (RhA-B) dye on the surface of NiONPs. A dye solution containing RhA-B was mixed with NiO nanoparticles for a period of 30 min while being agitated. Using a double beam UV-visible spectrophotometer at the maximum absorption wavelength of the dye ( $\lambda_{max} = 554$  nm), concentration variations in RhA-B solution were measured and analyzed. Eqn. 2 was used to determine the amount of RhA-B that was adsorbed on the surface of NiONPs and eqn. 3 was used to determine the percentage of dye that was removed.

$$q_e = \frac{C_o - C_e}{M} \times V \quad (2)$$

$$\text{Removal (\%)} = \frac{C_o - C_e}{C_o} \times 100 \quad (3)$$

where  $C_o$  is the initial concentration of the adsorbate (mg/L);  $C_e$  is the equilibrium concentration of the solution (mg/L);  $V$  is the volume of the adsorbate solution (L) and  $M$  is the mass of the adsorbent (NiONPs) used (g).

**Langmuir isotherm model:** The Langmuir isotherm model is based on the intermolecular forces that could decrease rapidly with the distance and the predicted monolayer sorption of the adsorbate on the active site of adsorbent. Langmuir isotherm is expressed in eqn. 4. The plot of  $C_e/q_e$  versus  $C_e$  was analyzed to calculate the Langmuir isotherm parameters at room temperature.

$$q_e = q_m K_L \frac{C_e}{1 + K_L C_e} \quad (4)$$

The linear form of the above equation is:

$$\frac{C_e}{q_e} = \frac{1}{K_L} q_m \left( \frac{1}{q_m} \right) C_e \quad (5)$$

where  $C_e$  is the equilibrium concentration (mg L<sup>-1</sup>),  $q_e$  is the amount adsorbed per gram of adsorbent (mg g<sup>-1</sup>),  $K_L$  is the Langmuir equilibrium constant related to the energy of adsorption and  $q_m$  (mg g<sup>-1</sup>) is the monolayer adsorption capacity. The  $q_m$  and  $K_L$  values were calculated from the slope and intersection of  $C_e/q_e$  versus  $C_e$  plots. The Langmuir isotherm can be expressed as a dimensionless constant called the parameter of the equilibrium constant  $R_L = 1/(1 + K_L C_o)$ , where  $K_L$  is the Langmuir constant and  $C_o$  is the maximum initial dye concentration in mg/L.

**Freundlich's isotherm model:** The Freundlich's isotherm model is based on adsorption on the non-uniform surfaces and assumes that adsorption occurs at active sites of adsorbents with different energies. The Freundlich's constants  $K_F$  and  $n$  are related to the adsorption capacity and adsorption strength, respectively. This model can be generalized as:

$$\ln q_e = \left( \frac{1}{n} \right) \ln C_e \ln K_F \quad (6)$$

**Temkin's isotherm model:** Temkin's isotherm describes the interaction between adsorbent and adsorbate, which could explain the linear decrease in heat of adsorption of the molecules on the adsorbent surface layer. The adsorption potentials of the adsorbent for adsorbate can be determined using the Temkin's adsorption isotherm model [21]. The Temkin's isotherm can be generalized as follows:

$$q_e = \left( \frac{RT}{b} \right) \ln K_T C_e \quad (7)$$

The linear form of the above equation becomes:

$$q_e = B \ln KT + B \ln C_e \quad (8)$$

where  $K_T$  is the equilibrium binding constant (L/g),  $B$  (J/mol) is a constant related to the heat of adsorption which is calculated

from the relation  $B = RT/b$ , where  $R$  is the gas constant (8.314J/mol/K) and  $T$  is the absolute temperature (K).

**Kinetic study:** Adsorption kinetics was studied using pseudo-first-order and pseudo-second-order kinetic models. A pseudo-first-order model can be represented as follows [22]:

$$\frac{dq}{dt} = k_1 (q_e - q_t) \quad (9)$$

where  $q_e$  and  $q_t$  are the adsorbed masses in mg/g at equilibrium and time  $t$ , respectively;  $K_1$  (min<sup>-1</sup>) is the rate constant of the first-order kinetic equation. The integral form of the above equation can be written as:

$$\log q_e = \log(q_e - q_t) - \frac{k_1}{2.303t} \quad (10)$$

At 25 °C,  $k_1$  was calculated from the slope of graph between  $\log(q_e - q_t)$  versus  $t$  and the  $q_e$  from the intercept. Adsorption data for NiO-600 was analyzed using a pseudo-second-order kinetic equation. The second-order rate equation can be expressed as [23]:

$$\frac{dq}{dt} = k_2 (q_e - q_t)^2 \quad (11)$$

where  $k_2$  (mg<sup>-1</sup>min<sup>-1</sup>) is the pseudo-second-order adsorption rate constant. The integral form of the above equation can be formulated as:

$$\frac{t}{q_t} = \frac{1}{k_2 q_e^2} + \frac{1}{q_e t} \quad (12)$$

The values of  $q_e$  and  $k_2$  can be determined from the slope and intersection of the straight line plot of  $t/q_t$  versus  $t$ .

## RESULTS AND DISCUSSION

**UV studies:** The nickel oxide nanoparticles (NiONPs) were isolated from *Phyllanthus emblica* fruit extract and used to remove the textile pigment rhodamine B (RhA-B) dye by adsorption in an effort to reduce water pollution. The prepared nanoparticle was characterized by various analytical techniques. Calcined NiONPs at 70, 200, 400 and 600 °C were examined by UV absorption spectrum. Although no significant peaks were observed and particle size reduction causes a shift of the absorption band towards lower wavelengths with increase in temperature [24-26]. Using the absorption data, Tauc polt was obtained between the photon energy (hv) vs. quantity  $(\alpha hv)^{1/2}$ . According to the findings (Fig. 1a-b), the energy of band gap in NiONPs at 600 °C is 5.74 eV (70 °C), 5.75 eV (200 °C), 5.96 eV (400 °C) and 5.98 eV (600 °C), respectively. As the calcination temperature increased, the optical band gap of NiONPs also increased. This relation indicates a decrease in particle size with respect of the band gap [27].

**FTIR studies:** As seen in Fig. 2, the FT-IR spectrum of NiONPs possess a number of prominent absorption bands. The Ni-O stretching vibrational mode is responsible for the broad absorption band at 600 cm<sup>-1</sup> and the breadth of the absorption band signifies a less preventable quality of NiONPs. The O-H stretching vibration was found to be responsible for the broad absorption band at 3395 cm<sup>-1</sup> and the -C=O stretching

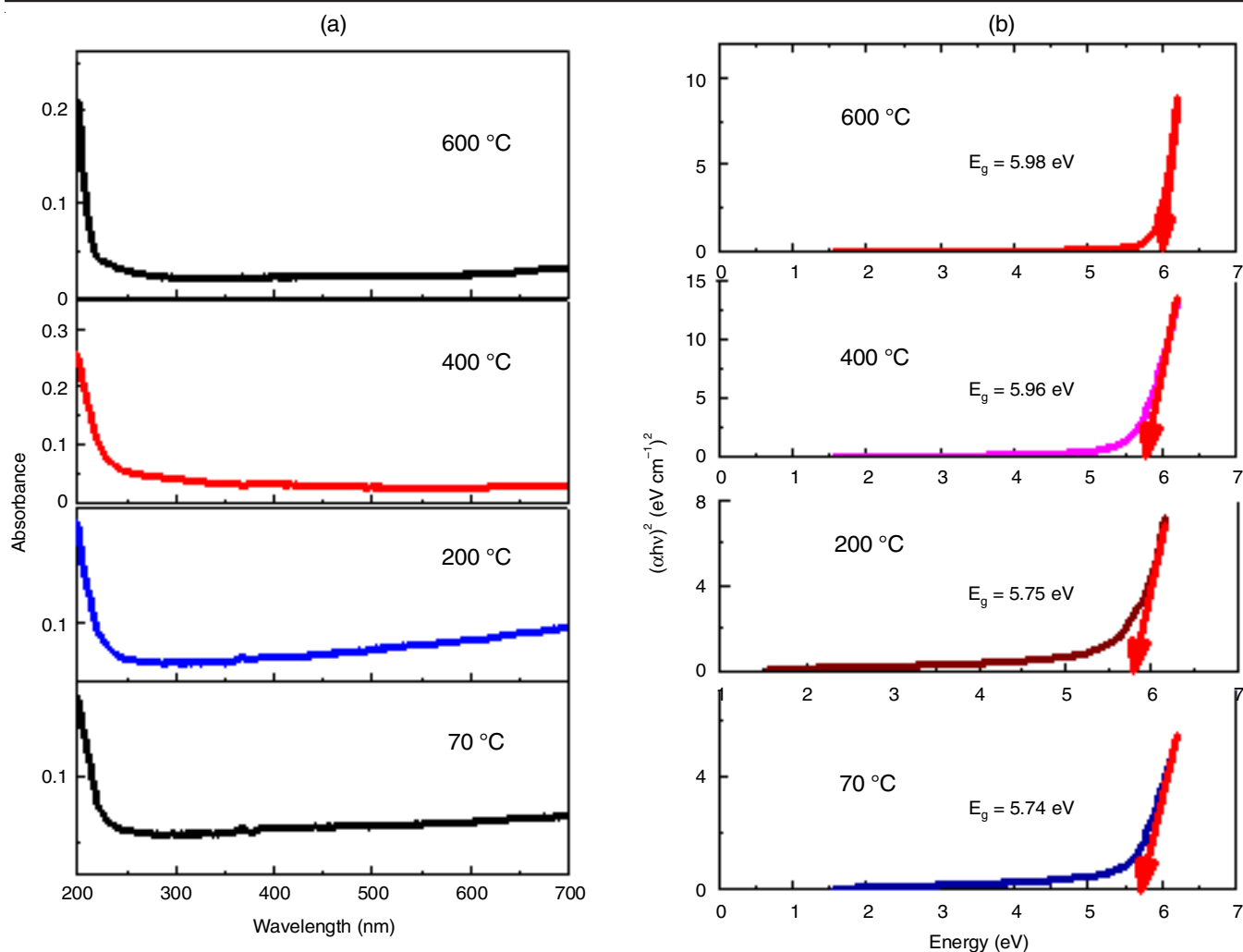


Fig. 1. (a) UV-visible spectra, (b) Tauc plot of NiONPs calcined at different temperatures

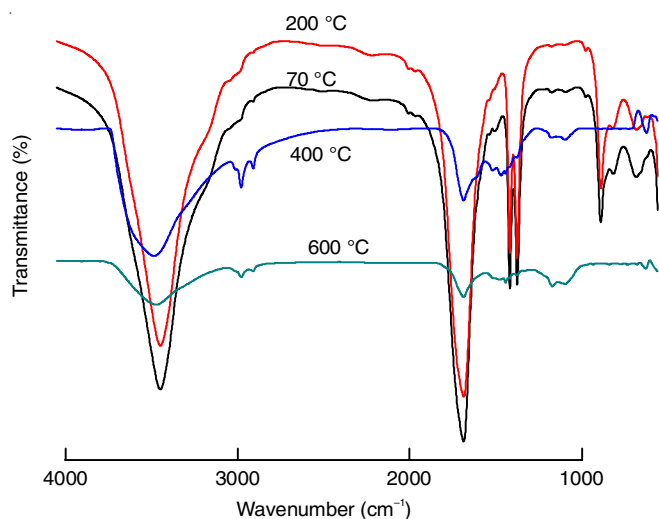


Fig. 2. FTIR spectrum of NiONPs calcined at different temperatures

vibration mode was found to be responsible for the sharp band at 1600 cm<sup>-1</sup> [28]. The significance of the impact that water has on the structure was demonstrated by these observations. On the other hand, this finding may potentially imply the existence of hydroxyls in NiONP calcined at 70 °C. The sharp absorption

at 750 cm<sup>-1</sup> is attributed to the tensile vibrations. The absorption bands at 1500-1300 cm<sup>-1</sup> region were assigned to the symmetric and asymmetric O-C=O stretching vibrations and C-O stretching vibrations, indicating that Ni may exist as an oxalate form, NiC<sub>2</sub>O<sub>4</sub>·2H<sub>2</sub>O at 70 °C and 200 °C. These peaks were diminished at 400 °C and 600 °C indicated that nickel oxalate was converted to NiONPs.

**Morphology studies:** The FE-SEM images of NiO-70 and NiO-600 are shown in Fig. 3. It is evident that the resulting NiONPs formed agglomerated clusters of spherical, large and heterogeneous nanoparticles. Also, the dissimilar shape and size of NiO-70 could be a result of a non-uniform nucleation process. This aggregation can be caused by the generally large surface area and high surface area to unit volume ratio [29]. The FESEM images of NiO-600 exposed uniform and coarse nanoparticles. The average particle size of NiO-70 and NiO-600 was 5 μm and 50 nm, respectively. The UV, FTIR and SEM analysis outcomes are almost coincidence with the reported values of reported work of Uddin *et al.* [24].

Further, the nanoparticle nature was confirmed by HR-TEM analysis and the image of NiO-600 are shown in Fig. 4. From the image, this work observed tubular shape (10 nm) for NiO-600 and confirmed the nanoparticles nature.

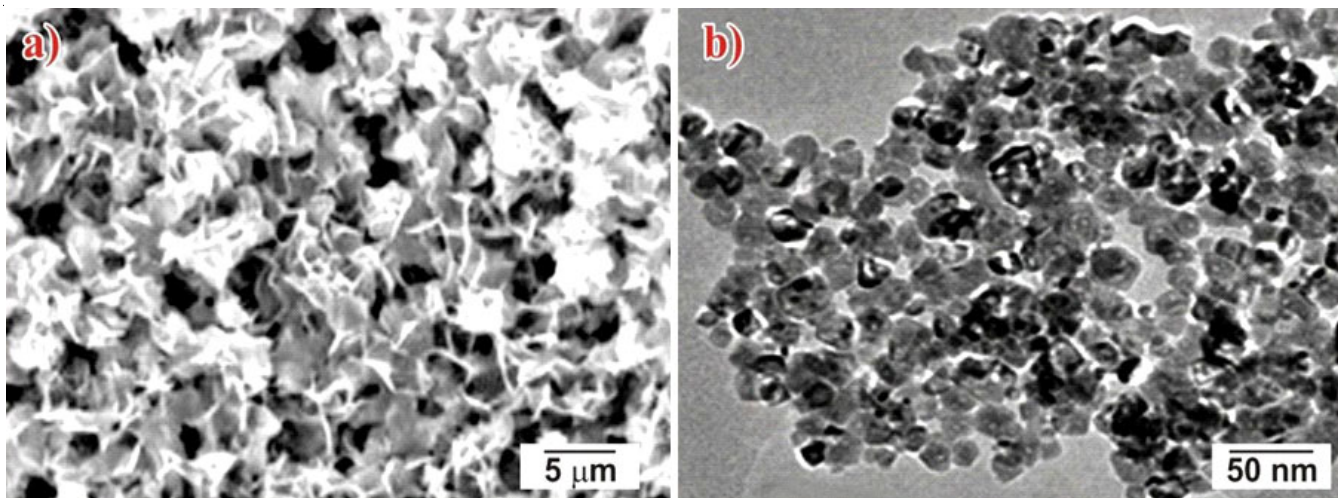


Fig. 3. FESEM images of (a) NiO-70 and (b) NiO-600

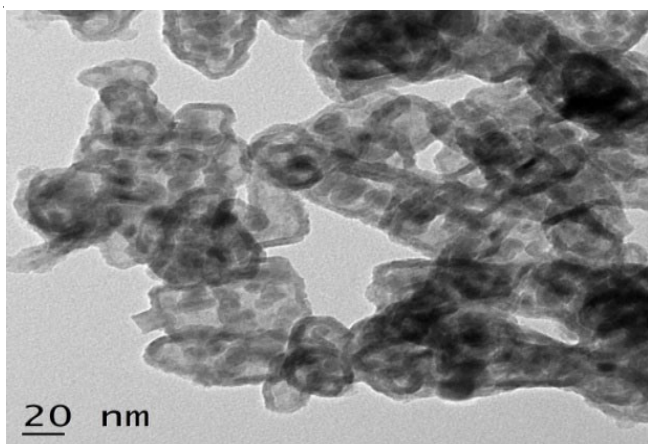


Fig. 4. HRTEM image NiO-600

**Thermal studies:** In the TGA curve (Fig. 5a), three mass losses were observed for NiO-70 at 228 °C (I), 359 °C (II) and 500 °C (III). It demonstrates that the stoichiometry of the sample changes with increasing sample preparation tempe-

perature and that weight loss is negligible at > 600 °C. The weight loss at 228 °C and 359 °C was accompanied by sharp DTA peaks as shown in Fig. 5b.

The weight loss at 228 °C is due to the dehydration of water molecules and impurities in NiONPs. The weight loss at 359 °C is related to the decomposition of nickel oxalate into NiO. The weight loss can be explained as due to the thermal decomposition of nickel oxalate to form NiO particles [30].

**Batch studies:** Among the various synthesized NiONPs, NiO-70, NiO-200, NiO-400 and NiO-600, the characterization studies showed that NiO-600 was more homogeneous and had smaller spherical nanoparticles. Therefore, NiO-600 was used as an effective adsorbent to remove RhA-B dye from the aqueous solution. As the number of adsorbent increases, the removal of RhA-B also increases up to 0.1 g of adsorbent and the adsorption of dye by the adsorbent is stable (Fig. 6a-b). A maximum removal rate of 90% was observed at an adsorbent capacity of 0.1 g for NiO-600. This may be due to the higher availability of adsorption sites at higher adsorbent dosages. An increase in the adsorbent removal rate may be associated with a large

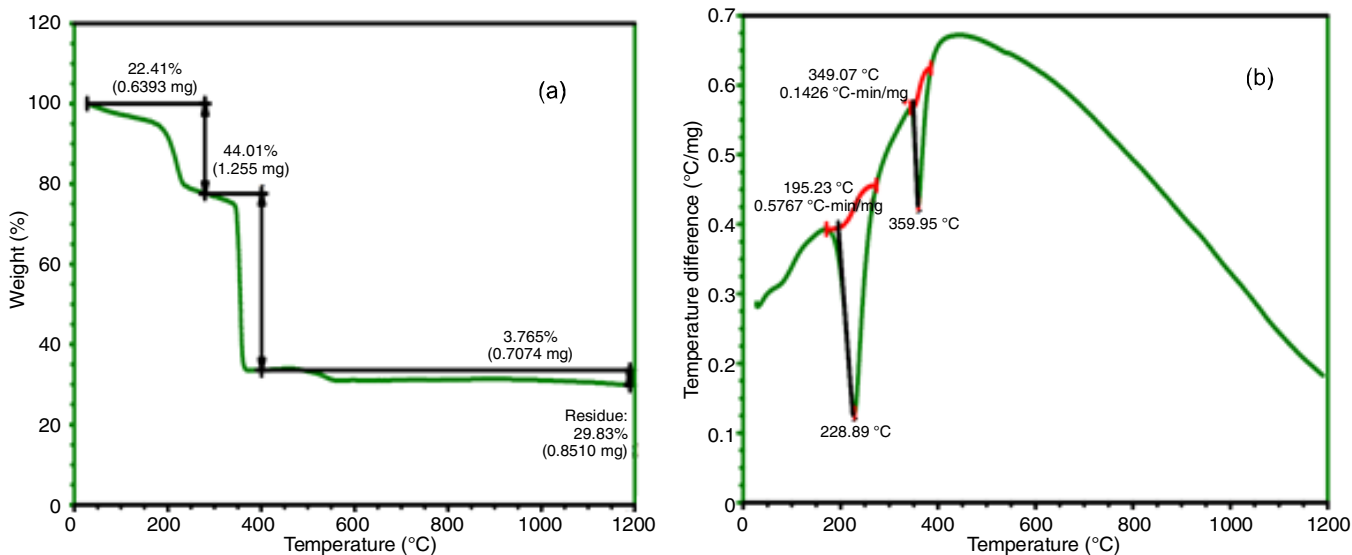


Fig. 5. Thermal curves (a) TGA, (b) DSC curves of NiO-600 nanoparticles

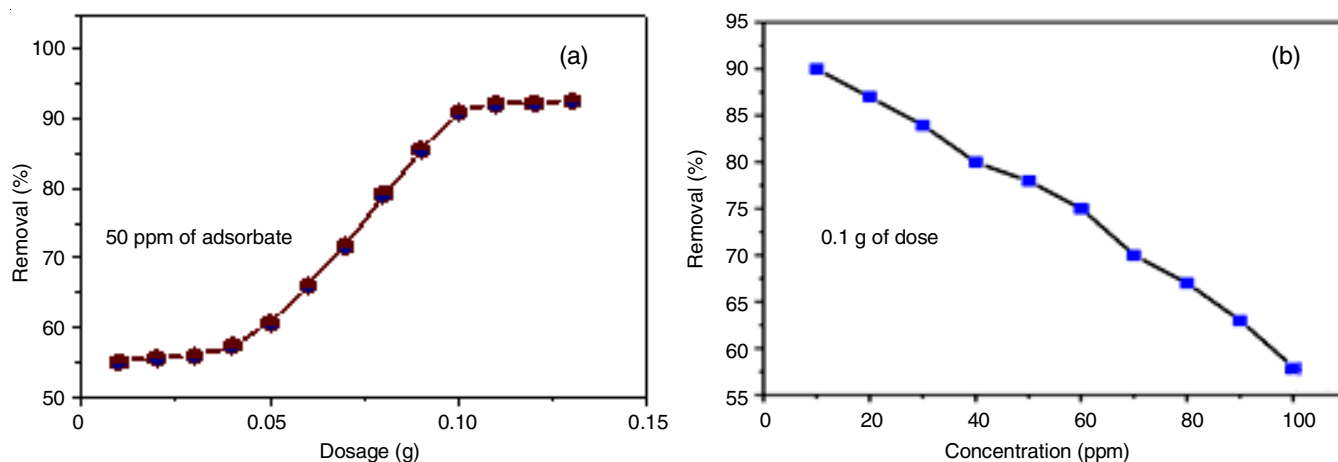


Fig. 6. Effect of dosage of adsorbent (a) and adsorbate (b) concentrations

TABLE-1  
 ADSORPTION RESULT WITH RESPECT OF ADSORBENT AND ADSORBATE CONCENTRATIONS

| Batch experiment using NiONPs-600 with RhA-B |                      |             |  |
|--|----------------------|-------------|--|
| NiONP dosage                                 | Initial conc. of dye | Removal (%) | Response   |
| 0.01 g to 0.1 g                              | 50 ppm               | 90          | Gradual increase until the equilibrium state and then constant |
| 0.1 g/100 mL                                 | 10 to 100 ppm        | 85          | Gradual decrease   |

specific surface area that can provide adequate reactivity and active adsorption centers [31]. The adsorption outcomes are shown in Table-1.

**Adsorption studies:** The adsorption capacity of rhodamine B (RhA-B) dye on NiO-600 was studied using different adsorption isotherms. In this study, the Langmuir, Freundlich and Temkin isothermal models were used to investigate the relationship between the amount and concentration of adsorbed RhA-B and the parameters obtained are shown in Table-2. The  $K_L$  values calculated were in the range of 0–1, indicating a good adsorption process ( $0 < R_L < 1$ ) for the obtained NiO-600 and the obtained range exists between 0.3 and 0.6, indicating that the adsorption process of the obtained adsorbent was good. Similarly, Freundlich's isotherm results showed that increasing the negative charge on the surface increased the electrostatic force between the NiONPs and thus increase the adsorption of RhA-B. The 'n' values were found to be 0.7-0.8, indicating strong adsorption of RhA-B dye on the NiO-600 surface. The extent of adsorption will be indicative of the binding energy between RhA-B and NiO-600, and thus the possibility of chemisorption rather than physical adsorption. It was known that the constants  $K_T$  and B would be high for good adsorbents and low for poor adsorbents. Therefore, it is possible for the Temkin isotherm to be successfully adapted by the adsorption of RhA-B. Correlation coefficients ( $R^2$ ) were used to determine which model best described the adsorption process. The  $R^2$  is closer to 1, the better the fit between the experimental data and the data predicted by the model is the best fit. Comparing  $R^2$  of each isotherm of Langmuir (0.980.99), Freundlich (0.980.99) and Temkin (0.970.99) for NiO-600, it can be seen that almost all the isotherms are most suitable for RhA-B adsorption, which suggests both homogeneous and heterogeneous monolayer adsorption processes in which all adsorption sites have the same affinity for the adsorbate.

TABLE-2  
 ADSORPTION ISOTHERM PARAMETERS FOR  
 THE UPTAKE OF RhA-B ONTO NiO-600

| Temp. (K) | Langmuir isotherm   |              |        |
|-----------|---------------------|--------------|--------|
|           | $q_m$ (mg/L)        | $K_L$ (mg/g) | $R^2$  |
| 303       | 355.87              | 0.5995       | 0.9933 |
| 313       | 328.94              | 0.5458       | 0.9863 |
| 318       | 465.11              | 0.3126       | 0.9944 |
|           | Freundlich isotherm |              |        |
|           | n                   | $K_F$ (mg/g) | $R^2$  |
| 303       | 0.8338              | 1.6405       | 0.9887 |
| 313       | 0.7431              | 6.7344       | 0.9824 |
| 318       | 0.7997              | 38.2912      | 0.9947 |
|           | Temkin isotherm     |              |        |
|           | $K_T$ (L/g)         | B (J/mol)    | $R^2$  |
| 303       | 1.0668              | 98.2794      | 0.9967 |
| 313       | 1.0223              | 117.3031     | 0.9737 |
| 318       | 1.0276              | 177.9512     | 0.9967 |

The maximum monolayer adsorption ( $q_m$ ) obtained from the Langmuir plot was 328-465 mg/L. The  $K_F$  (1.6-38.2) and n (0.70.8) values were calculated from the Freundlich's isotherm and the  $K_T$  (1.02-1.07) and B values calculated from the Temkin's isotherm indicate favourable chemisorption of RhA-B on NiO-600.

**Kinetic studies:** The calculated  $q_e$  values from the pseudo-first-order and pseudo-second-order kinetic models agreed well with the experimental  $q_e$  values. Table-3 showed the adsorption behaviour, the pseudo-second-order kinetic models very well. The  $k_2$  value of the pseudo-second order model was higher in NiO-600 ( $2.0495 \times 10^{-2} \text{ mg}^{-1} \text{ min}^{-1}$ ).

**Thermodynamic studies:** The standard free energy change ( $\Delta G^\circ$ ) for the adsorption of RhA-B onto NiO-600 was calculated using eqn. 14:

| Kinetic models      | Parameters                                 | NiO-600                 |
|---------------------|--|-------------------------|
| Pseudo-first-order  | $k_1$ ( $\text{min}^{-1}$ )                | $2.3083 \times 10^{-5}$ |
|                     | $q_e$ (mg/g)                               | 4.0197                  |
|                     | $R^2$                                      | 0.9009                  |
| Pseudo-second-order | $k_2$ ( $\text{mg}^{-1} \text{min}^{-1}$ ) | $2.0495 \times 10^{-2}$ |
|                     | $q_e$ (mg/g)                               | 3.5236                  |
|                     | $R^2$                                      | 0.9884                  |

$$K_d = \frac{q_e}{C_e} \quad (13)$$

$$\Delta G^\circ = -RT \ln K_d \quad (14)$$

where  $\Delta G^\circ$  is the Gibbs free energy change (KJ/mol); T is the temperature (K); R is the gas constant (8.314 J/mol/K) and  $K_d$  is the equilibrium constant related to Langmuir constant equal to  $q_e/C_e$ . The calculated  $\Delta G^\circ$  was found to be -79.00 KJ/mol and confirmed the spontaneity of the monolayer adsorption process [32]. The higher negative value confirmed the feasibility of adsorption as a chemisorption process. The results also revealed that the adsorption was endothermic.

**Recycling studies:** The adsorbed RhA-B dye molecules were easily desorbed using tap water and distilled water (an appropriate amount of acetone) with magnetic stirring for 1 h. Thus, in order to investigate the secondary pollution of RhA-B dye in different environments, after the adsorption process, six cycles of successive desorption experiments were conducted as shown in Fig. 7. The desorption of RhA-B was found to be increased with the number of cycles whereas the recovery of adsorbent was found to be 89, 85, 80, 78, 75 and 70% after the first, second, third, fourth, fifth and sixth cycles, respectively. The results showed that as the number of cycles increased, the recovery of the adsorbent gradually both in water and acetone for NiO-600 recovery decreased from 89% to 70%. Desorption efficiency was 70% after six cycles were calculated as follows:

$$\text{Desorption efficiency (\%)} = \frac{\text{Amt of desorbed RhA-B}}{\text{Amt of adsorbed RhA-B}} \times 100$$

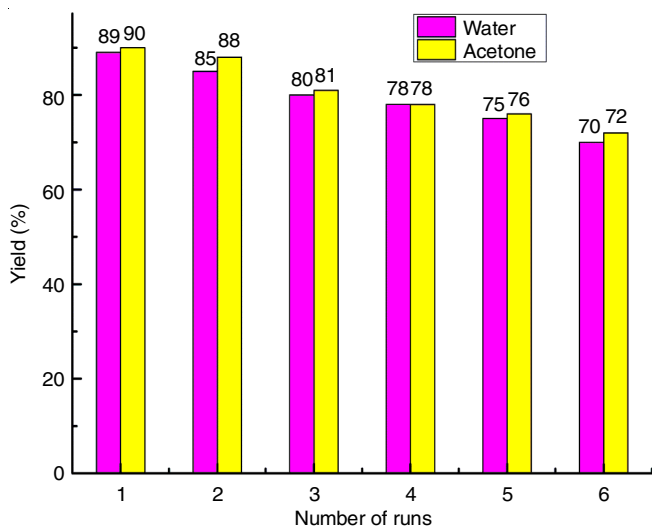


Fig. 7. Desorption studies of rhodamine B due

It was suggested that such adsorbent not only possesses a high adsorption capability but also presented a good desorption efficiency for RhA-B dye. The maximum adsorption capacity and high desorption rate would be the advantages of this type of adsorbent and thus NiONPs has been proposed as an effective adsorbent to reduce purification costs.

**Comparison studies:** The efficiency of the green synthesized NiONPs were compared with the other reported NiO nanoparticles dye towards the removal of RhA-B dye. As per Table-4, this work observed that the adsorption and photocatalytic efficiency of the current green synthesized NiO nanoparticles were increased with time and doped materials. Thus, the removal efficiency of *Phyllanthus emblica* fruit extract based NiO nanoparticles was almost equal with the reported values. Despite the fact that we were successful in removing the pigment from NiO nanoparticles in 70 min, while the other reported NiO nanoparticles have indicated that this process can take significantly longer. Also, the doped NiO nanomaterials showed lower efficiency when compared to present green synthesized NiO nanomaterials. Hence, this work claims the low cost higher efficiency NiONPs using *Phyllanthus emblica* fruit extract for the dye removal purpose in textile industry effluent treatment.

TABLE-4  
COMPARISON OF PREPARED NiONP EFFICIENCY WITH REPORTED VALUES

| Adsorbent      | Adsorbate     | Time (min) | Removal (%) | Ref.          |
|----------------|---------------|------------|-------------|---------------|
| NiONP          | Methyl orange | 30         | 95          | [33]          |
| NiONP          | Waste water   | 120        | 50          | [34]          |
| NiONP + ZnO    | RhA-B         | –          | 93.8        | [35]          |
| NiONP          | RhA-B         | –          | 81          | [35]          |
| Ag-Cd + NiONP  | RhA-B         | –          | 97          | [36]          |
| NiONP          | RhA-B         | –          | 80.33       | [37]          |
| Ag doped NiONP | RhA-B         | 200        | 75          | [38]          |
| NiONP (green)  | RhA-B         | 30×60      | 95          | [39]          |
| NiONP          | RhA-B         | 70         | 95          | Present study |

## Conclusion

This study conducts the successful preparation of nickel oxide nanoparticles (NiONPs) by green synthesis using nickel chloride hexahydrate and *Phyllanthus emblica* fruit extract and calcined at high temperatures. The synthesized NiONPs were characterized by UV, FTIR, FESEM, TEM and TGA/DTA. The green NiONPs has the cubic structure and a calculated size of 50 nm. Experimental data from the Langmuir, Freundlich and Temkin isotherms showed that the equilibrium data fit best. The high negative of free energy indicates that the adsorption is chemisorption and spontaneous. The NiO nanoparticles eliminated RhA-B dye from the water sample upto 88% at pH 6.

## CONFLICT OF INTEREST

The authors declare that there is no conflict of interests regarding the publication of this article.

## REFERENCES

- M.F. Hou, C.X. Ma, W.D. Zhang, X.Y. Tang, Y.N. Fan and H.F. Wan, *J. Hazard. Mater.*, **186**, 1118 (2011); <https://doi.org/10.1016/j.jhazmat.2010.11.110>
- K.P. Singh, S. Gupta, A.K. Singh and S. Sinha, *Chem. Eng. J.*, **165**, 151 (2010); <https://doi.org/10.1016/j.cej.2010.09.010>
- D.Y. Lei, B. Li, Q. Wang, B. Wu, L. Ma and H. Xu, *Desalination Water Treat.*, **54**, 2794 (2015); <https://doi.org/10.1080/19443994.2014.904817>
- X. Dong, W. Ding, X. Zhang and X. Liang, *Dyes Pigments*, **74**, 470 (2007); <https://doi.org/10.1016/j.dyepig.2006.03.008>
- M. Berradi, R. Hsissou, M. Khudhair, M. Assouag, O. Cherkaoui, A. El Bachiri and A. El Harfi, *Heliyon*, **5**, e02711 (2019); <https://doi.org/10.1016/j.heliyon.2019.e02711>
- T. Shindhal, P. Rakholiya, S. Varjani, A. Pandey, H.H. Ngo, W. Guo, H.Y. Ng and M.J. Taherzadeh, *Bioengineered*, **12**, 70 (2021); <https://doi.org/10.1080/21655979.2020.1863034>
- M. Vakili, M. Rafatullah, B. Salamatinia, A.Z. Abdullah, M.H. Ibrahim, K.B. Tan, Z. Gholami and P. Amouzgar, *Carbohydr. Polym.*, **113**, 115 (2014); <https://doi.org/10.1016/j.carbpol.2014.07.007>
- T. Ahmad, M. Rafatullah, A. Ghazali, O. Sulaiman and R. Hashim, *J. Environ. Sci. Health Part C Environ. Carcinog. Ecotoxicol. Rev.*, **29**, 177 (2011); <https://doi.org/10.1080/10590501.2011.601847>
- V. Gupta, O. Moradi, I. Tyagi, S. Agarwal, H. Sadegh, R. Shahryari-Ghoshekandi, A. Makhlof, M. Goodarzi and A. Garshasbi, *Crit. Rev. Environ. Sci. Technol.*, **46**, 93 (2016); <https://doi.org/10.1080/10643389.2015.1061874>
- D. Rickerby and M. Morrison, *Sci. Technol. Adv. Mater.*, **8**, 19 (2007); <https://doi.org/10.1016/j.stam.2006.10.002>
- H. Sadegh, G.A.M. Ali, V.K. Gupta, R. Shahryari-Ghoshekandi, A.S.H. Makhlof, M.N. Nadagouda, M. Sillanpää and E. Megiel, *J. Nanostruct. Chem.*, **7**, 1 (2017); <https://doi.org/10.1007/s40097-017-0219-4>
- E.A. Dil, M. Ghaedi and A. Asfaram, *Ultrason. Sonochem.*, **34**, 792 (2017); <https://doi.org/10.1016/j.ultsonch.2016.07.015>
- A.T. Hoang, S. Ni•etic, C.K. Cheng, R. Luque, S. Thomas, T.L. Banh, V.V. Pham and X.P. Nguyen, *Chemosphere*, **287**, 131959 (2022); <https://doi.org/10.1016/j.chemosphere.2021.131959>
- J. Li, R. Yan, B. Xiao, D.T. Liang and D.H. Lee, *Energy Fuels*, **22**, 16 (2008); <https://doi.org/10.1021/ef700283j>
- Z. Wei, T. Xia, L. Bai, J. Wang, Z. Wu and P. Yan, *Mater. Lett.*, **60**, 766 (2006); <https://doi.org/10.1016/j.matlet.2005.10.008>
- D. Sivaselvi, N. Vijayakumar, R. Jayaprakash, A. Venkatesan, B. Kartha, P.K. Senthilkumar, M. Nicoletti, N.S. Alharbi, S. Kadaikunnan, J.M. Khaled and M. Govindarajan, *J. Drug Deliv. Sci. Technol.*, **69**, 103160 (2022); <https://doi.org/10.1016/j.jddst.2022.103160>
- N. Vijayakumar, V.K. Bhuvaneshwari, G.K. Ayyadurai, R. Jayaprakash, K. Gopinath, M. Nicoletti, S. Alarifi and M. Govindarajan, *Saudi J. Biol. Sci.*, **29**, 2270 (2022); <https://doi.org/10.1016/j.sjbs.2021.11.065>
- S. Ying, Z. Guan, P.C. Ofoegbu, P. Clubb, C. Rico, F. He and J. Hong, *Environ. Technol. Innov.*, **26**, 102336 (2022); <https://doi.org/10.1016/j.eti.2022.102336>
- P. Devaraj, P. Kumari, C. Aarti and A. Renganathan, *J. Nanotechnol.*, **2013**, 1 (2013); <https://doi.org/10.1155/2013/598328>
- M.I. Din, M. Tariq, Z. Hussain and R. Khalid, *Nano-Metal Chem.*, **50**, 292 (2020); <https://doi.org/10.1080/24701556.2019.1711401>
- M. Vadi, A.O. Mansoorabadi, M. Mohammadi and N. Rostami, *Asian J. Chem.*, **25**, 5467 (2013); <https://doi.org/10.14233/ajchem.2013.14786>
- A. Bhatnagar, E. Kumar, A.K. Minocha, B.H. Jeon, H. Song and Y.C. Seo, *Sep. Sci. Technol.*, **44**, 316 (2009); <https://doi.org/10.1080/01496390802437461>
- Shivangi, S. Bhardwaj and T. Sarkar, *J. Taiwan Inst. Chem. Eng.*, **113**, 223 (2020); <https://doi.org/10.1016/j.jtice.2020.08.011>
- S. Uddin, L.B. Safdar, J. Iqbal, T. Yaseen, S. Laila, S. Anwar, B.A. Abbasi, M.S. Saif and U.M. Quraishi, *Microsc. Res. Technol.*, **84**, 2004 (2021); <https://doi.org/10.1002/jemt.23756>
- Z. Sabouri, A. Akbari, H.A. Hosseini, M. Khatami and M. Darroudi, *Green Chem. Lett. Rev.*, **14**, 404 (2021); <https://doi.org/10.1080/17518253.2021.1923824>
- E. Saion, E. Gharibshahi and K. Naghavi, *Int. J. Mol. Sci.*, **14**, 7880 (2013); <https://doi.org/10.3390/ijms14047880>
- N.M. Hosny, *Polyhedron*, **30**, 470 (2011); <https://doi.org/10.1016/j.poly.2010.11.020>
- Y.-L.T. Ngo and S.H. Hur, *Mater. Res. Bull.*, **84**, 168 (2016); <https://doi.org/10.1016/j.materresbull.2016.08.004>
- M.M. Hussain, M.M. Rahman and A.M. Asiri, *J. Environ. Sci.*, **53**, 27 (2017); <https://doi.org/10.1016/j.jes.2016.03.028>
- S. Rakshit, S. Ghosh, S. Chall, S.S. Mati, S.P. Moulik and S.C. Bhattacharya, *RSC Adv.*, **3**, 19348 (2013); <https://doi.org/10.1039/c3ra42628a>
- F. Falaki and A. Fakhri, *J. Phys. Theor. Chem. IAU, Iran*, **10**, 255 (2014).
- H.A. Al-Aoh, *Desalination Water Treat.*, **110**, 229 (2018); <https://doi.org/10.5004/dwt.2018.22223>
- Q. Riaz, M. Ahmed, M. N. Zafar, M. Zubair, M. F. Nazar, S. H. Sumrra, I. Ahmad and A.H. Bandegharaeic, *Int. J. Environ. Anal. Chem.*, **102**, 84 (2022); <https://doi.org/10.1080/03067319.2020.1715383>
- R. Nateghi, G.R. Bonyadinejad, M.M. Amin and H. Mohammadi, *Int. J. Environ. Health Eng.*, **1**, 25 (2012); <https://doi.org/10.4103/2277-9183.98384>
- S. Jolaei, M. Mirzaei, A. Hassanpour, H.H. Safardoust and A. Khani, *J. Nanostruct.*, **12**, 761 (2022); <https://doi.org/10.22052/JNS.2022.03.029>
- M. Shakil, U. Inayat, M. Tanveer, G. Nabi, S.S.A. Gillani, M. Rafique, N.H. Tariq, A. Shah and A. Mahmood, *Int. J. Environ. Sci. Technol.*, **20**, 2021 (2023); <https://doi.org/10.1007/s13762-022-04101-2>
- S.D. Khairnar and V.S. Shrivastava, *J. Taibah Univ. Sci.*, **13**, 1108 (2019); <https://doi.org/10.1080/16583655.2019.1686248>
- S. Ghazal, A. Akbari, H. A. Hosseini, Z. Sabouri, F. Forouzanfar, M. Khatami and M. Darroudi, *Appl. Phys. A* **126**, 480 (2020); <https://doi.org/10.1007/s00339-020-03664-6>
- M. Saheb, H.A. Hosseini, A. Hashemzadeh, B. Elahi, L. Hasanzadeh, R.K. Oskuee and M. Darroudi, *ChemistrySelect*, **4**, 2416 (2019); <https://doi.org/10.1002/slct.201803903>